Sensing-Based Correlation Analysis of Surface Elevation and Topsoil Depth in Japanese Rice Paddy Field

Eiji MORIMOTO, Jaehwan LEE, Kazuto NISHIDA and Hiromichi ITOH

Kobe University, Japan

A paper from the Proceedings of the

17th International Conference on Precision Agriculture and 11th Brazilian Congress on Precision and Digital Agriculture

13-15 July 2026

Porto Alegre, Brazil

Abstract.

This study conducted a grid-based correlation analysis of surface elevation and topsoil depth (TD) in a 1.4 ha rice paddy field using a 2 meter grid. A UAV collected 34,080,826 surface elevation data points, while a smart rice transplanter measured 8,021 TD points. Offset correction minimized missing TD data to 2.2% within the grid. A weighted RMSE optimized the grid size, balancing spatial homogeneity and local variability. Analysis revealed a negative correlation between surface elevation and TD (r = −0.53), indicating that lower elevations generally correspond to deeper topsoil.

Keywords.

topsoil depth, field surface elevation, grid-based correlation analysis, weighted RMSE, smart rice transplanter

Introduction

According to the "Japan Soil Inventory" provided by the National Agriculture and Food Research Organization (NARO) (2019), Gley Lowland soils, which are widely distributed across rice paddy zones in Japan, have a high groundwater table and remain in a reduced state. Consequently, the layer within 50 cm from the surface is prone to water saturation throughout the year. It has been pointed out that excessive moisture conditions resulting from poor drainage can adversely affect the growth, yield, and quality of rice (Kohyama, 1993). Similarly, Terasawa (1975) highlighted the importance of drainage management in rice cultivation, reporting that waterlogged conditions inhibit root respiration and nutrient absorption in rice, thereby leading to poor growth. Therefore, proper management of soil moisture conditions in paddy fields is indispensable for stable rice production.

In recent years, establishing new management methods has been demanded to respond to variations in soil physical properties within large-scale plots. Kuwabara et al. (2021) investigated the impacts on the physical properties of topsoil and subsoil in paddy fields and reported that it is desirable for the subsoil to fall within the pF range of 2.0 to 2.5. However, limitations in conventional management methods have also been identified; for instance, Osari et al. (2004) reported that insufficient compaction during land leveling operations using bulldozers causes differential settlement, presenting a settlement risk that reaches up to 70% within two months from the start of construction. These previous studies demonstrate the importance of management based on soil physical properties in large-scale fields, making it crucial to understand the factors influencing changes in these properties.

On the other hand, as research clarifying the specific effects of field management on the growth and quality of paddy rice, Sasaki et al. (2002) found that even in relatively level, large paddy fields (where most points fall within ±0.05 m of the average elevation), slight height variations on the field surface show a negative correlation with initial plant height. Furthermore, they revealed that, particularly depending on water management conditions, the emergence rate of tillers on upper nodes decreases at lower surface points, showing a significant positive correlation with the elevation of the paddy field surface (hereinafter referred to as surface elevation), thereby affecting tiller securement.

Furthermore, Matsunaga et al. (2018) investigated the effects of tillage depth and slow-release fertilizers on the yield and quality of "Hinohikari" rice, clarifying that shallow tillage (0.1 m) resulted in an immature grain rate of up to 16.3%, tending to degrade appearance quality compared to standard (0.15 m) or deep tillage (0.2 m). These studies indicate that field management practices, such as surface elevation and tillage depth, exert critical influences on the growth and quality of paddy rice.

The aforementioned factors—soil moisture conditions, physical properties, surface elevation, and tillage depth—do not only independently influence rice growth, but are also deeply interrelated, forming a complex growth environment. For example, tillage depth and field surface flatness dictate the physical characteristics of the plow layer, which directly impacts soil permeability and water retention—namely, the soil moisture status. Additionally, the state of the soil physical properties affects the difficulty of appropriate water management. In this manner, the growth environment of rice in paddy fields is multi-dimensionally defined by the physical characteristics of the soil and the fundamental field geometry, such as surface elevation and topsoil depth. Therefore, to comprehensively understand these factors and optimize field management, it is extremely critical to efficiently and accurately collect topographical and soil information representing the baseline state of the field and to comprehend its spatial variations.

However, conventional manual topographical and soil surveys require a substantial amount of time and labor for large-scale areas, leading to reduced efficiency and decreased data reliability due to human error (Komine et al., 1980). As reported by Kanda et al. (2023), even when constructing soil group prediction models using machine learning, limitations such as duplicating collected data to compensate for the shortage of soil survey data have become apparent. Therefore, to realize wide-area topographical and soil surveys, a high-density collection method capable of gathering data in a short time is required.

As a method for measuring surface elevation, which constitutes the topographical information of a field, UAV technology has been reported to be effective because it can survey extensive terrain in a short period (Islam et al., 2020). Nakayama et al. (2020) pointed out that remote sensing technology using UAVs is rapidly spreading across various fields such as agriculture, river management, and disaster recovery. In particular, studies by Sakai et al. (2021), Nomura et al. (2021), and Yamashita et al. (2022) reported that a UAV system equipped with a green laser of 532 nm wavelength enables the construction of Digital Elevation Models (DEMs) including water bodies. UAV technology has been proven to be an effective tool for measuring extensive and complex topographical data, even in areas that are difficult to access.
Meanwhile, Morimoto et al. (2013) developed a system capable of collecting and measuring topsoil depth data using a soil-sensor-mounted variable-rate fertilizer rice transplanter (hereinafter referred to as a smart rice transplanter). The topsoil depth sensor mounted on the smart rice transplanter utilizes an ultrasonic distance sensor, which calculates the distance to the field surface from the round-trip time of sound waves, and subsequently derives the topsoil depth based on the sinkage amount of the vehicle body. Since the measurements by the topsoil depth sensor correlated with the actual measured values with a coefficient of determination of $R^2 = 0.99$, they reported that topsoil depth can be measured effectively.
Therefore, based on the surface elevation and topsoil depth data collected using a UAV and a smart rice transplanter, this study aimed to clarify the following two objectives: (1) Proposing a method for optimizing the grid cell size to appropriately evaluate spatial variations within a field. (2) Analyzing the spatial correlation between surface elevation and topsoil depth, and investigating the feasibility of utilizing spatial information for field management.

Material and Method

1. Method of Collecting Surface Elevation Data

As shown in Fig. 1, drone surveying using a UAV (Matrice 600 Pro, DJI) and a green laser scanner (hereinafter referred to as TDOT3, Amuse Oneself) was applied to collect surface elevation data. Furthermore, correction data were collected based on electronic reference points using RTK-GNSS, and the distance to the field surface was measured with the TDOT3.
(Fig. 1)

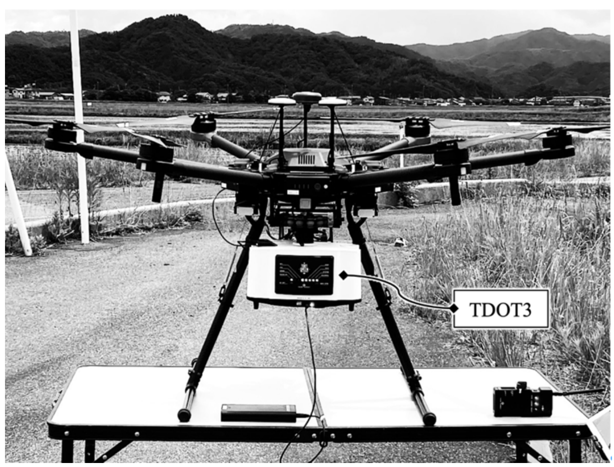

Fig. 1 UAV sensing system

The survey site was an experimental field (1.4 ha rice paddy, Gley Lowland soil) located in Iwami Town, Tottori Prefecture, and data for DEM generation were collected based on the "Public Survey Manual" of the Geospatial Information Authority of Japan (GSI) (2018).

(1) Flight Settings and Measurement

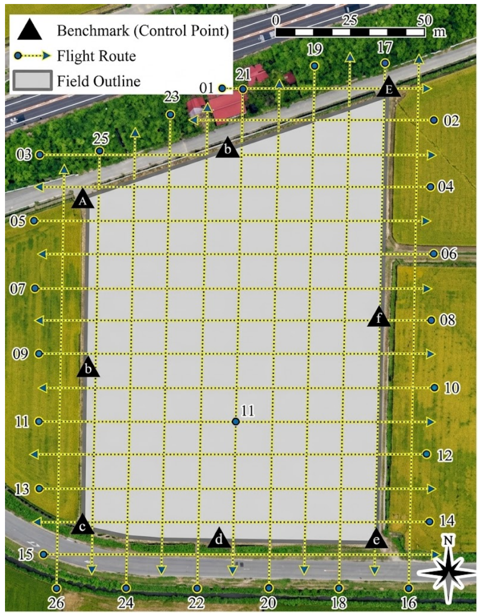

Fig. 2 UAV flight route and survey area map

According to Mano et al. (2020), the TDOT3 has a maximum measurement distance of 158 m (at 10% reflectivity) and a measurement accuracy of ±15 mm. Moreover, it has a measurement rate of 30,000 points/s, enabling the measurement of high-density point cloud data exceeding 100 points/m². In this study, to protect eyesight from the laser beam of the TDOT3, the flight altitude of the UAV was set to 40 m, considering the Nominal Ocular Hazard Distance (NOHD). The flight route was established as shown in Fig. 2, and the 3D point cloud data of the field were collected via autonomous flight under conditions of a wind speed of 2.0 m/s and a temperature of 21 °C. The overlap rate at this time was 75%.

(2) Surveying Adjustment Control Points and Data Integration

For the point cloud data collected by the UAV, spatial distortions are corrected using dedicated data processing software for the TDOT3 (TDOT PROCESSING, Amuse Oneself) based on the RTK-GNSS and IMU data obtained during the flight. Furthermore, to guarantee the accuracy of the height information of the point cloud data, the coordinates of the adjustment control points were surveyed using an electronic reference point (Iwami A, 3.3 km away from the experimental field) and a total station. Elevation was calculated by applying a geoid model to the ellipsoidal height obtained via RTK-GNSS, and the surface elevation data were corrected, converted into a plane rectangular coordinate system (EPSG:2447), and saved in LAS format.

Using the above method, a total of 34,080,826 3D point cloud data points were collected through a UAV laser survey conducted on June 8, 2022, the day before the rice transplanting operation. Furthermore, based on the surface elevation information extracted from this 3D point cloud data, statistical parameters of the surface elevation were calculated to quantitatively evaluate the irregularity characteristics of the experimental field. These indices serve as baseline data to understand the surface conditions of the field and to perform comparative discussions with the characteristics of typical rice paddy fields.

2. Method of Collecting Topsoil Depth Data

An 8-row smart rice transplanter (PRJ8-FV, Iseki & Co., Ltd.) was used to collect topsoil depth data. As shown in Fig. 3, ultrasonic sensors (UM30-213113, SICK) were installed on the front left and right sides of the transplanter at an installation height of 850 mm, with a sensor spacing of 1,500 mm.

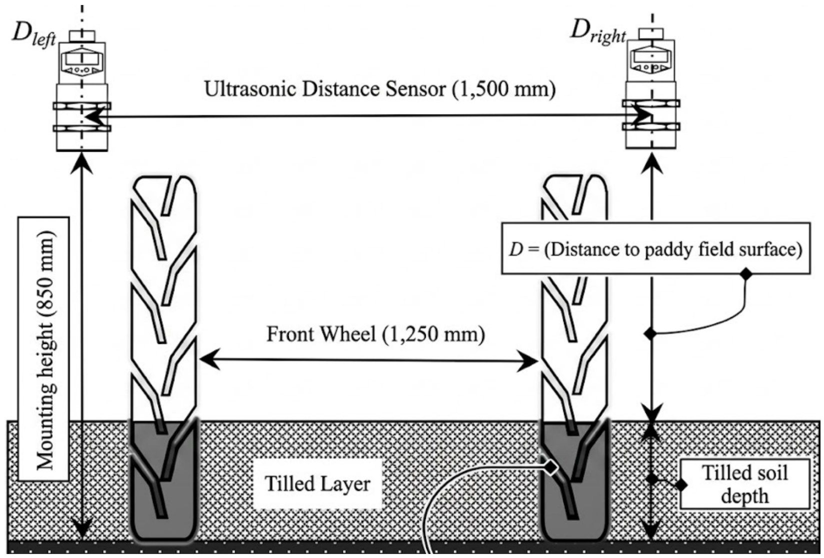

Fig. 3 Method of measuring topsoil depth using ultrasonic distance

The distances to the field surface were measured by the left and right sensors (D_{left}, D_{right}) , and the difference between the installation height and the average of those distances was calculated as the topsoil depth (Eq. (1)). Simultaneously, location information was recorded at a frequency of 1 Hz using a DGPS (A100, Hemisphere), integrated with the sensor measurement data, and

$$\text{Topsoil Depth} = 850\ (\text{mm}) - \frac{D_{left} + D_{right}}{2} \quad (1)$$

saved in CSV format.
The collection of topsoil depth data was conducted simultaneously with the transplanting operation, which was carried out in a drained state after puddling. On June 9, 2022, 8,021 data points were collected during this operation using the smart rice transplanter.

3. Derivation of the Data Augmentation Method Based on Offset
The smart rice transplanter is equipped with a single GPS antenna, which collects the coordinates of the center of the machine body. Therefore, if the grid cell size is smaller than the full width of the transplanter (2,400 mm), grid cells with no plotted data may occur. In this study, a data augmentation method utilizing an offset process was applied to resolve this issue.
(1) Method of Calculating Azimuth
To obtain the azimuth of the traveling direction of the transplanter, the azimuth was calculated using the GPS coordinates of two consecutive points, as shown in Fig. 4. The GPS coordinates of the start point are defined as $(\lambda_1,\ \phi_1)$ and the coordinates of the end point as $(\lambda_2,\ \phi_2)$. For latitude, north latitude is positive and south latitude is negative; for longitude, east longitude is positive and west longitude is negative. The azimuth θ is determined using the longitude difference $\Delta\lambda = \lambda_2 - \lambda_1$ indicates the direction from the start point to the end point, and when $\Delta\lambda$ is 0, both points are located on the same meridian, representing north or south (Veness, 2002).

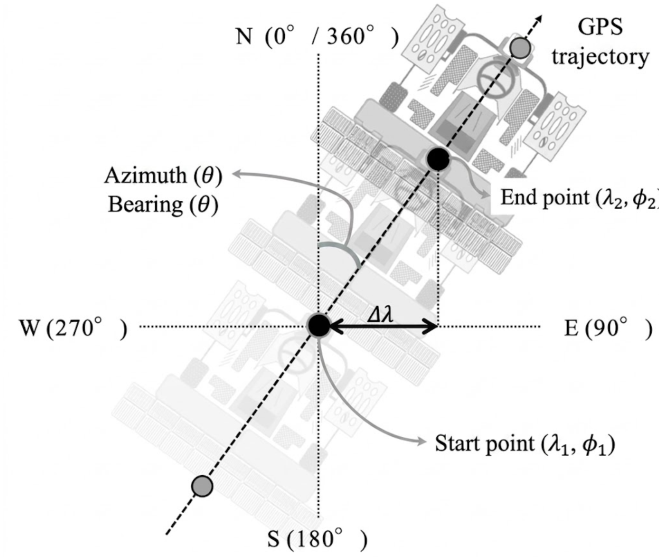

Fig. 4 Method of calculating the azimuth

A method based on the law of cosines in spherical trigonometry is used to calculate the azimuth. First, the x-component and y-component are calculated from the latitudes ϕ_1, ϕ_2 and the longitude difference $\Delta\lambda$, and the azimuth θ is obtained using Eq. (2) via the atan2 function, which takes these components as arguments.

$$\theta = \operatorname{atan} 2\left(\frac{\cos(\phi_2)\sin(\Delta\lambda)}{\cos(\phi_1)\sin(\phi_2) - \sin(\phi_1)\cos(\phi_2)\cos(\Delta\lambda)}\right) \tag{2}$$

Unlike the standard atan function, the atan2 function used here receives two arguments (the x-component and y-component) simultaneously and performs the calculation by considering their respective sign information. For this reason, it can accurately distinguish the second and third quadrants, which cannot be differentiated by $\operatorname{atan}(x)$, and possesses the characteristic of returning a unique angle within the range from $-\pi$ to π. Consequently, it enables the calculation of azimuth across all directions and is widely adopted as a standard method in the fields of navigation and positioning (Gade, 2010; Miura, 2015; IOGP, 2019).

(2) Data Augmentation by Offset Processing

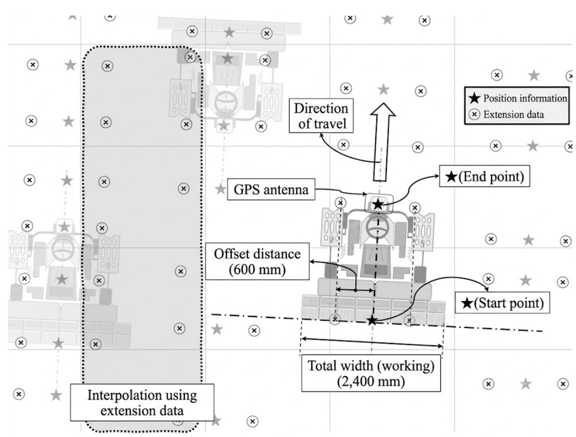

Fig. 5 Conceptual diagram of GPS coordinate offset

As shown in Fig. 5, using the collected GPS coordinates and the azimuth θ calculated by Eq. (2), the horizontally offset position coordinates were computed to augment the data. Specifically, points offset by a distance corresponding to 1,200 mm (half of the working width) to the left and right directions at 90° relative to the traveling direction from the position of the GPS antenna were designated as augmented data. The geodesic function included in the geopy library of Python 3 was utilized to calculate these offset coordinates. This function computes the destination latitude and longitude by taking the start latitude and longitude, the azimuth $\theta \pm 90^\circ$, and the distance (1.2 m) as inputs. This generated augmented data corresponding to the entire working width of the rice transplanter, complementing the data deficiency within the grid cells.

4. Optimal Selection of Cell Size and Grid Analysis Method

In spatial data analysis, cell size exerts a critical impact on the spatial detail and accuracy of the analysis results. If the cell size is too small, missing data increase (Webster et al., 2007), whereas if it is too large, local variations are less likely to be reflected (Li et al., 2008). De Smith et al. (2007) pointed out the influence of cell size selection on accuracy.

Based on these considerations, this study aimed to thoroughly examine the effects of cell size on analysis results, introduce grid analysis to handle both surface elevation and topsoil depth at the identical spatial scale, and establish a method to determine the optimal cell size. To determine the cell size k based on the topsoil depth data, which has a lower density between the two datasets, grid analysis was performed from 1 m to 5 m in 1 m increments, and the cell size was determined from the results using the RMSE and missing rate as evaluation indices.

(1) Method of Calculating RMSE of Topsoil Depth Data Using Q-Q Plots

To quantitatively evaluate the impact of grid processing on the statistical characteristics of the original data, this study constructed percentile-based Q-Q plots and compared the distribution shapes between the original data and the grid data of each cell size (1 to 4 m). In the process of gridding, multiple original data points are aggregated within a cell, which causes a loss of spatial reproducibility with the original data, making direct comparison between identical positions difficult. Therefore, it was determined that a method focusing on the distribution characteristics of the entire dataset and comparing them based on the correspondence of percentile values would be effective.

A Q-Q plot is a technique to visually and quantitatively evaluate the reproducibility of distributions by comparing values corresponding to each percentile between two datasets (Sayama, 2018). Specifically, the original data and the grid data were each sorted in ascending order, and corresponding percentile values were extracted to create the plots. Additionally, the number of percentiles was set to N=100 to enable a detailed comparison of the data distribution in 1% increments.

Furthermore, the Root Mean Square Error (RMSE) was calculated based on the differences between the percentile values obtained from the Q-Q plot. This RMSE is an index that numerically represents differences in distribution shapes, and it was used to evaluate to what extent different cell sizes can preserve the distribution characteristics of the data, serving as a criterion for selecting the optimal cell size.

(2) Evaluation Indices for Selecting the Optimal Cell Size

Shinoda et al. (2019) stated that the RMSE, which evaluates the difference between observed and predicted values, treats all data points equally, making it difficult to evaluate specific data characteristics. On the other hand, Nakai et al. (2022) reported that a Weighted RMSE, which applies weights to errors, can improve accuracy under specific conditions. Therefore, the Missing Rate Weighted RMSE (MRWRMSE), which integrates the RMSE and the missing rate (hereinafter m_k), was introduced, and the cell size that minimized the MRWRMSE was defined as the optimal solution. Here, m_k was calculated using Eq. (3).

$$m_k = \frac{n_{missing}}{N_{total}} \tag{3}$$

Here, $n_{missing}$ denotes the number of cells where no data exist, and N_{total} represents the total number of cells at cell size k. Next, the MRWRMSE was calculated using Eq. (4).

$$\mathrm{MRW_{RMSE}} = \frac{\sqrt{\frac{1}{n}\sum_{i=1}^{n}(o_i - p_i)^2}}{(1 - m_k)} \tag{4}$$

Here, o_i and p_i indicate the values corresponding to the *i*th percentile of the original data and grid data, respectively, and n represents the total number of data pairs. The term $(1 - m_k$ uses the proportion of cells containing data as a weight to correct the RMSE calculated from the Q-Q plot.

(3) Grid Analysis

Leutenegger et al. (1997) showed that the STR-tree (Sort-Tile-Recursive Tree) is a method that efficiently partitions spatial geometry, achieving reductions in search time and savings in computational resources. The grid analysis of surface elevation and topsoil depth data was processed using the STR-tree function of the Shapely library in a Python 3 environment. Both the field perimeter polygon in GeoJSON format and the datasets in CSV format were partitioned by the cell size k, and the average of the values plotted within a cell was designated as the representative value for each cell.

5. Correlation Analysis between Surface Elevation and Topsoil Depth

Based on the grid maps created through the grid analysis, the mean surface elevation and mean topsoil depth in each cell were calculated, and the correlation between both variables was analyzed. It has been suggested that spatial analysis of topographical data is effective for understanding natural environmental factors such as soil moisture, solar radiation, and vegetation distribution (Aoki, 1986; Hirata, 2005).

Through the correlation analysis of surface elevation and topsoil depth, the spatial variation within the field was elucidated, and the usefulness of topsoil depth information as baseline data for appropriate tillage operations was clarified. First, the mean values for each cell and the overall averages of surface elevation and topsoil depth were calculated, and the correlation coefficient r was determined using Eq. (5). Based on r, the correlation between both variables was quantitatively evaluated, and a scatter plot was generated to visualize their relationship.

$$r = \frac{\sum_{i=1}^{n}(x_i - \bar{x})(y_i - \bar{y})}{\sqrt{\sum_{i=1}^{n}(x_i - \bar{x})^2}\sqrt{\sum_{i=1}^{n}(y_i - \bar{y})^2}} \quad (5)$$

Here, x_i and y_i represent the mean values of surface elevation and topsoil depth in the i-th cell, respectively, and $\bar{x}$ and $\bar{y}$ denote the overall mean values of both variables.

Results and Discussion

1. Results of Data Collection

(1) Surface Elevation Data

The surveying accuracy of the collected 3D point cloud data for surface elevation was verified. As a result of obtaining the absolute errors against the coordinates of 8 adjustment control points measured via RTK-GNSS, the errors in the horizontal (XY) directions were 0.004 m and 0.01 m, respectively, and the error in the vertical direction (Z) was 0.01 m. Furthermore, the mean value of the surface elevation was 0.91 m, the standard deviation was 0.02 m, and the maximum height difference was 0.09 m. This demonstrated that the TDOT3 can quantitatively evaluate minute irregularities on the field surface.

In particular, in a previous study, Sasaki et al. (2002) defined a field falling within a range of ±0.05 m relative to the average elevation as a "relatively level, large-scale rice paddy field," while reporting that even in such fields, slight height differences of several centimeters affect the growth of paddy rice. The maximum height difference of the experimental field in this study falls within the range of this "relatively level" criterion, indicating that it does not possess particularly large irregularities compared to general paddy fields. However, taking the indications of the aforementioned study into account, even the level of irregularities shown by this experimental field could potentially influence rice growth. Furthermore, this can be considered a field characteristic that warrants sufficient discussion when analyzing the spatial relationship with topsoil depth, which is the main subject of this study.

The average data density calculated from the collected 34,080,826 3D point cloud data points was approximately 2,434 points/m², indicating that high-density point cloud data were successfully collected. Therefore, the adopted flight plan and sampling rate were judged to be appropriate for the purpose of comprehending detailed surface geometry in this study.

(2) Topsoil Depth Data

The number of collected topsoil depth data points was 8,021. This is the result of collecting data while traveling across 41 passes within the field under conditions where the actual average operating speed v_{avg} was 0.9 m/s and the sampling rate S_{rate} was 1 point/s.

Assuming an effective working width of 2.4 m, the theoretical minimum travel distance L_{min} to completely cover the experimental field is 5,900 m. Under these conditions, the minimum required number of data points P_{min} was calculated using Eq. (6), yielding 6,555 points.

Therefore, the collected 8,021 data points correspond to approximately 1.2 times D_{min}. This indicates that a necessary and sufficient data density and spatial coverage were achieved to analyze the spatial variation of topsoil depth in detail, including necessary overlapping operations within the field and data collection during turning at headlands.

$$P_{min} = \frac{L_{min}}{v_{avg}} \times S_{rate} \tag{6}$$

The mean value, standard deviation, minimum value, and maximum value of the topsoil depth data were 0.2 m, 0.04 m, 0.1 m, and 0.3 m, respectively, confirming spatial variations within the field. Therefore, for the purpose of understanding the topsoil depth distribution across the entire field in more detail, the data were augmented through the offset process, resulting in an augmented dataset of 16,042 points, which is twice the size of the original data.

2. Determination of the Optimal Cell Size

(1) Grid Analysis by Cell Size

Table 1 shows the results of calculating $N_{total},\ n_{missing}\ and\ m_k$ for each cell size by conducting grid analysis using the augmented topsoil depth dataset. At a cell size of 1 m, N_{total} was 13,662 cells, $n_{missing}$ was 5,702 cells, and m_k was 0.417. As the cell size increased, m_k decreased sharply. Then, when the cell size reached 4 m or larger, m_k became 0. On the other hand, the surface elevation had an m_k of 0 at all cell sizes.

Table 1 Total cell count and missing rate for each cell size of topsoil depth data

Cell size (m)	N_{total}	$n_{missing}$	m_k
1	13,662	5,702	0.417
2	3,411	68	0.019
3	1,526	4	0.002
4	864	0	0.000
5	559	0	0.000

These results indicate that the surface elevation data possess an extremely high data density compared to the topsoil depth data. In addition, for the topsoil depth data, $n_{missing}$ increases when the cell size is less than 4 m. Consequently, data interpolation becomes necessary in grid analysis, which may decrease the reliability and representativeness of the spatial distribution.

(2) Calculation of RMSE for Topsoil Depth Data Using Q-Q Plots

As a result of comparing the distributions between the original data and the grid data of each cell size (1 m to 4 m) using Q-Q plots for the topsoil depth data, it was confirmed that clear differences in reproducibility occurred depending on the cell size. Fig. 6 shows the results of the RMSE calculated from the Q-Q plots up to a cell size of 4 m. At a cell size of 1 m, the RMSE showed the minimum value of 0.0108 m, indicating the highest reproducibility of the distribution compared to the original data. However, because $n_{missing}$ was large and m_k also exhibited a high value of 0.42, it was revealed that challenges remained regarding data coverage. At a cell size of 2 m, m_k decreased to 0.019, improving the missing data issue, but the RMSE increased to 0.0116 m, showing a slight decrease in distribution reproducibility compared to the 1 m cell. Furthermore, at cell sizes of 3 m and 4 m, m_k became nearly 0, resolving the missing cells, but the RMSE increased to 0.0121 m and 0.0125 m, respectively. This indicated a trend where it becomes more difficult to reproduce the detailed distribution characteristics of the original data as the cell size expands. Particularly at a cell size of 4 m, a trend where the data points on the Q-Q plot deviated significantly from the reference line y=x was prominently observed. This is presumed to be because gridding accompanied by cell size expansion averages out the local spatial variations of the original data; especially in locations with deep topsoil depth, the peak values are averaged with the surrounding relatively low values, making the grid data values smaller than the percentile values of the original data, thereby thinning out the detailed features of the distribution. From the above, although a cell size of 1 m can preserve local variations most accurately, it carries a risk of reducing data reliability due to the occurrence of missing cells. On the other hand, while a cell size of 4 m resolves the missing data issue, it was clarified that it cannot sufficiently reproduce the spatial variations of the original data. Therefore, from the perspective of balancing the preservation of distribution characteristics and the reduction of missing data, a cell size of 2 m is considered the most appropriate.

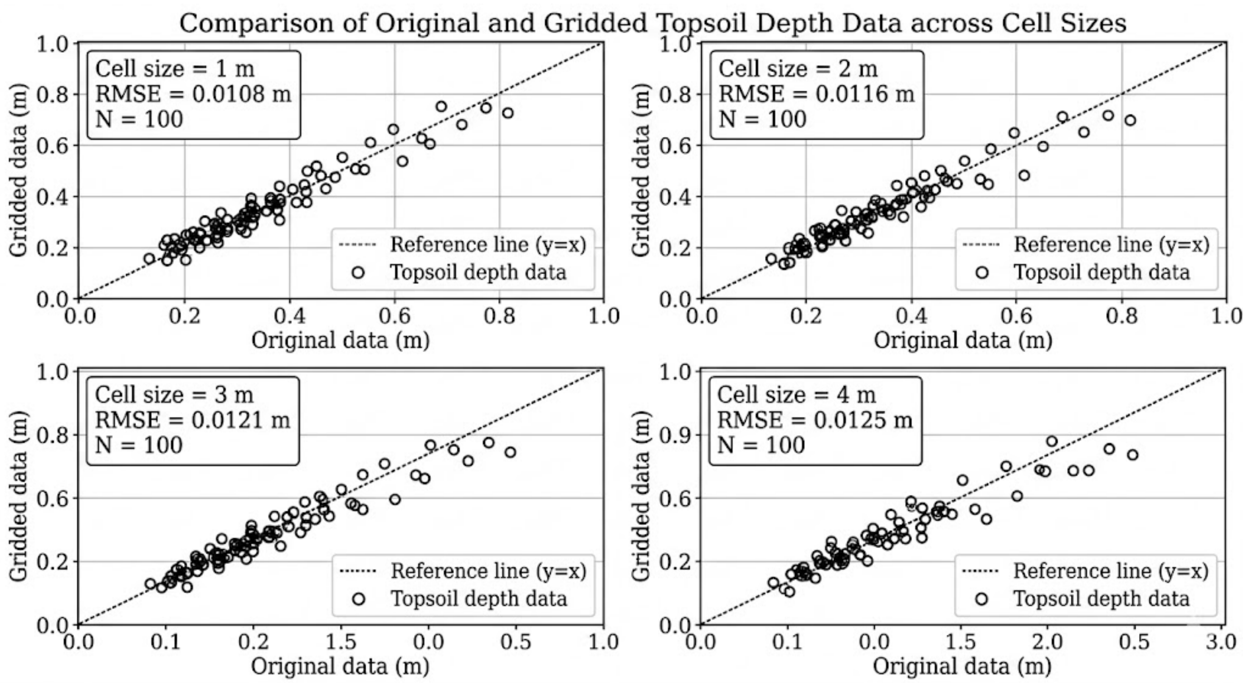

Fig. 6　Q-Q plot of topsoil depth data

(3) Selection of Optimal Cell Size via MRWRMSE

Fig. 7 shows the results of calculating the MRWRMSE to select the optimal cell size. At a cell size of 1 m, the MRWRMSE exhibited the highest value of 0.02 due to the influence of m_k. Conversely, at a cell size of 2 m, the MRWRMSE was at its minimum of 0.012, demonstrating that it is the optimal solution for capturing the spatial homogeneity and local variations of topsoil depth information.

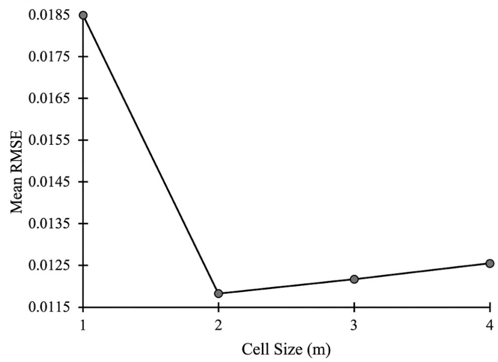

Fig. 7 MRW$_{RMSE}$ of four cell sizes

At cell sizes of 3 m and larger, the MRWRMSE tended to increase gradually. For instance, at cell sizes of 3 m and 4 m, the values were 0.0121 and 0.0125, respectively, and since m_k was 0, there was no variation in the RMSE. Therefore, for the analysis of topsoil depth data obtained by the smart rice transplanter with a full width of 2,400 mm, it was concluded that a cell size of 2 m, which showed the minimum MRWRMSE value, is optimal. This cell size can be said to optimally harmonize spatial resolution and data density with a favorable balance between m_k and RMSE.

3. Results of Grid Analysis

(1) Surface Elevation Data

Using the cell size of 2 m established by the MRWRMSE, grid analysis was conducted using the polygon created based on the field perimeter. As a result, the point density within each cell was 375 points/m², and the mean surface elevation was calculated as the representative value. The surface elevation data were analyzed uniformly within the polygon, creating a grid map with no missing data. As shown in Fig. 8(a), the 2 m cell grid map confirmed a trend where the surface elevation is relatively high on the northwest side of the field and low on the southeast side.

(2) Topsoil Depth Data

Grid analysis was performed on the topsoil depth data in the same manner as the surface elevation. At this time, as a result of processing using the augmented dataset, the missing rate, which was 18.8% before data augmentation, was significantly reduced to 2.2%, and the average point density within each cell became 1.3 points/m². From the topsoil depth grid map of a 2 m cell size shown in Fig. 8(b), a remarkable spatial variation in topsoil depth (within the range of 0.1 m to 0.3 m shown in the legend) across the entire field was clearly confirmed. Specifically, areas with relatively deep topsoil depth (indicated in red or orange, 0.25 m or deeper) were scattered in patches from the southeastern part to the central part of the field, while areas with shallow topsoil depth (indicated in blue or green, 0.15 m or shallower) spread across a portion of the northwestern and northeastern parts of the field. In this manner, a patch-like distribution pattern was formed throughout the field, confirming that local variations are large. For the correlation analysis described later, out of the total 3,411 cells, 3,343 cells were used, excluding 68 missing cells remaining on the map (black squares in the figure).

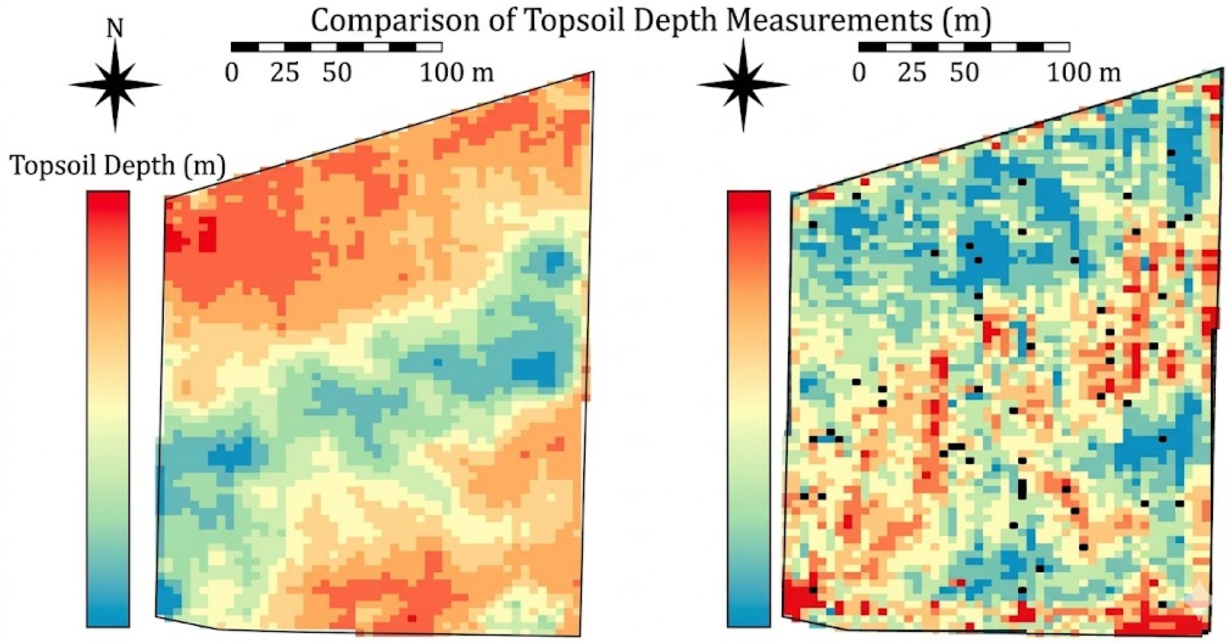

(a) (b)

Fig. 8 Grid analysis of (a) elevation and (b) topsoil depth

4. Correlation Analysis between Surface Elevation and Topsoil Depth

(1) Correlation Analysis and Its Factors

As a result of conducting a correlation analysis using the grid maps of surface elevation and topsoil depth, a statistically significant negative correlation was observed between the two variables (correlation coefficient $r = -0.53$, $p < 0.01$). As visually confirmed from the scatter plot shown in Fig. 9, it was clarified that locations with lower surface elevation tend to have deeper topsoil depth. This trend also matches the research report by Kawaharada et al. (2023). Behind this negative correlation, it is considered that repetitions of soil compaction and settlement due to long-term tillage operations and the traffic of agricultural machinery are involved. Due to these influences, minute height differences and spatial patterns of the physical properties of the plow layer may have been formed within the field.

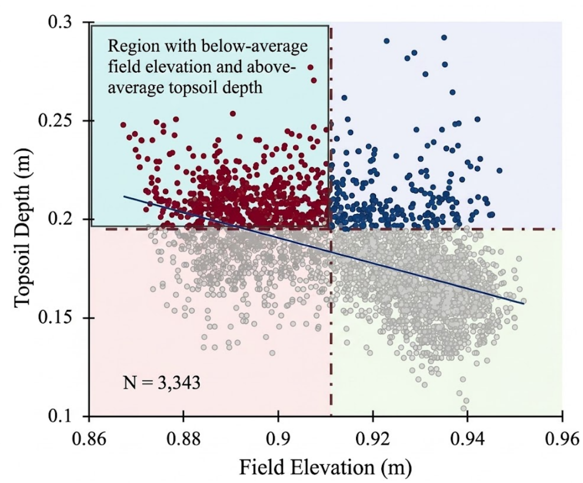

Fig. 9 Scatter plot of paddy field surface elevation and topsoil depth

Particularly, in locations where soil hardness below the ground surface has decreased due to deep tillage, the wheels of a tractor tend to sink more easily during operation. It is considered that through the repetition of such phenomena, zones characterized by relatively low surface elevation and deep topsoil depth were formed. However, various factors other than surface elevation are involved in the spatial variation of topsoil depth. For instance, soil movement during puddling, land subsidence, and local differences in the permeability or hardness of the plow sole layer can be cited. Clarifying the quantitative relationships between these multiple factors and surface elevation/topsoil depth is an important challenge for the development of precision tillage depth control technology and variable soil improvement techniques.

(2) Significance of Topsoil Depth Data and Feasibility of Utilizing Spatial Information

In this study, by utilizing the cell size selection method with the MRWRMSE as an evaluation index, datasets of different densities could be integrated and analyzed, appropriately capturing the spatial variations within the field. Through this analysis, it became possible to estimate the spatial distribution of surface water stagnation from the correlation between topsoil depth and surface elevation. For example, as shown in Fig. 10, a zone (a) with an average surface elevation of 0.91 m or lower was confirmed in the experimental field. Such zones are prone to water accumulation, which may lead to difficulties in drainage management and waterlogging of the soil. Additionally, the zone (b) with an average topsoil depth of 0.2 m or deeper was distributed within the low surface elevation zone (a). In the aerial photograph (c) taken by a drone immediately after rice transplanting, the zone indicated by the blue dashed line in the figure exhibits a darker brown color compared to the surroundings. This dark brown hue is considered to reflect surface water reflection caused by water stagnation. Thereby, it can be confirmed that the zone within the blue dashed line on the surface elevation and topsoil depth maps is in a water-stagnant state.

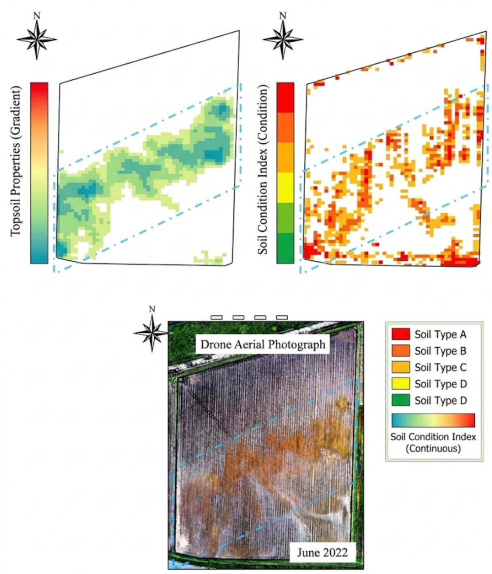

Fig. 10 Waterlogged areas inferred from elevation and topsoil depth

(3) Development toward Data-Driven Field Management and Future Outlook

The negative correlation between surface elevation and topsoil depth clarified in this study provides important knowledge for another objective of this research: "to obtain baseline information for data-driven field management by elucidating the spatial relationship between both datasets".

In particular, surface elevation data, which can be acquired extensively and at high density using a UAV, have the potential to be utilized as a clue to indirectly estimate the spatial trends of topsoil depth, which requires time and effort to measure. This information can contribute, for example, to selecting areas for intensive surveying or formulating precise field management plans using variable tillage depth and variable-rate fertilization. While it is known that the heterogeneity of the plow sole layer affects yield and quality, attempts to indirectly grasp its state and connect it to appropriate management will contribute to building a sustainable rice production system.

In the future, based on the spatial information of topsoil depth, it will be necessary to implement measures such as avoiding excessive deep tillage and introducing shallow tillage or no-till farming in deep zones. Conversely, in shallow zones, implementing soil improvement intensively through plow sole breaking or organic matter input can be cited; thus, the development of adaptive tillage depth control and soil management technologies corresponding to topsoil depth is an important challenge for the future.

IV Conclusion

In this study, utilizing a UAV and a smart rice transplanter, surface elevation and topsoil depth data were efficiently collected, and the relationship between the two was quantitatively clarified through grid analysis and correlation analysis. The primary achievements obtained are as follows:

1. Utilizing a UAV equipped with the TDOT3, 34,080,826 point cloud data points were collected, successfully acquiring detailed surface elevation data that included a maximum height difference of 0.09 m.
2. Using a smart rice transplanter, 8,021 topsoil depth data points were collected, and the number of data points was increased to 16,042 through offset-based data augmentation. In the case of a 2 m cell size, missing data were complemented by data augmentation, and as a result of data analysis for the transplanter with a full width of 2,400 mm, the missing rate was reduced from 18.8% to 2.2%.
3. As a result of grid analysis and correlation analysis, a statistically significant negative correlation ($r = -0.53$) was observed between surface elevation and topsoil depth. This indicates a trend where the topsoil depth becomes shallower as the surface elevation increases.

In addition, the optimal cell size was determined using the MRWRMSE, which weights the RMSE and the missing rate, as an evaluation index. As a result, it was demonstrated that a cell size of 2 m is the optimal solution for detailed visualization of local variations and the spatial homogeneity of topsoil depth information.

Acknowledgments

This work was supported by JSPS KAKENHI Grant Number JP24K01879, and received tremendous support in measurements from Mr. Yuzuru Maeda of S's Co., Ltd. We express our gratitude here.

References

De Smith, M. J., Goodchild, M. F., Longley, P., 2007. Geospatial analysis: A comprehensive guide to principles, techniques and software tools. Troubador Publishing Ltd., Market Harborough, UK, 1-491.

Gade, K., 2010. A non-singular horizontal position representation. The journal of navigation, 63(3), 395-417.

Islam, M. T., Yoshida, K., Sakai, K., Nishiyama, S., Tsuda, T., Nagata, K., Maeno, S., 2020. Model-induced comparative study of ALB and UAV-borne green LiDAR systems on vegetated lower Asahi River assessment in Japan. Journal of Japan Society of Civil Engineers, Ser. B1 (Hydraulic Engineering), 76(2), 529-534.

IOGP (International Association of Oil & Gas Producers), 2019, Geomatics Guidance Note Number 7, part 2. https://www.iogp.org/wp-content/uploads/2019/09/373-07-02.pdf. Accessed April. 1, 2025.